Journal of Hazardous Materials 176 (2010) 589–596

Contents lists available at ScienceDirect

Journal of Hazardous Materials

journal homepage: www.elsevier.com/locate/jhazmat

Hazardous gas releases in urban areas: Assessment of consequences through CFD modelling

M. Pontiggia[a], M. Derudi[a], M. Alba[b], M. Scaioni[b], R. Rota[a,*]

[a] Politecnico di Milano, Dipartimento di Chimica, Materiali e Ingegneria Chimica "Giulio Natta", via Macinelli 7, 20131 Milano, Italy
[b] Dipartimento di Scienza e Tecnologie dell'Ambiente Costruito (B.E.S.T.), via M. d'Oggiono 18/a, 23900 Lecco, Italy

ARTICLE INFO

Article history:
Received 1 September 2009
Received in revised form 2 November 2009
Accepted 12 November 2009
Available online 17 November 2009

Keywords:
CFD
Gas dispersion
Safety
Obstacles
Complex environments

ABSTRACT

Release of hazardous materials in urban areas is a major concern in industrial risk assessment. The presence of high population density in such areas multiplies the magnitude of the consequences. In urban areas, many buildings with complex geometries are involved leading to 3D flow fields that strongly influence gas dispersion. Representing such complex geometries simply but realistically in detailed simulation models can be cumbersome and often limit their utility. In this work, a methodology for the construction of 3D urban models and their importation into CFD models was developed through the access to spatial geodatabases, leading to a relatively fast and simple domain design technique. Moreover, since the magnitude of consequences depends on the absorbed dose which in turn depends on both concentration and exposure time, a simple methodology for dose evaluation was developed and implemented in a CFD code that enables the estimation of regions with a given death probability. The approach was developed and applied to a case study with different atmospheric stratification conditions. The results were then compared with those obtained using integral models. It was found that integral models can both overestimate and underestimate the magnitude of consequences related to hazardous material releases in urban areas.

1. Introduction

Accidents involving hazardous material releases constitute an important concern in industrial- and transport-related risk assessment. They can lead to consequences of large magnitude since the hazardous cloud can spread widely across distances of kilometres and pose a hazard to both human health and the environment.

Urban areas are easily involved in hazardous gas releases not only because many industries form part of urban agglomerations as a consequence of the growth of cities, but also because of the transport of hazardous materials by road and rail. The latter, while usually involving quantitatively smaller amounts of substances, still are a serious hazard both in terms of safety and security since their mitigation and prevention systems are less effective; moreover, transport vehicles transit through areas with highly vulnerable populations such as schools and hospitals. Besides, such incidents in urban areas present an extremely hazardous scenario in terms of the magnitude of consequences, exacerbated by the high population densities present in these areas.

Furthermore, urban areas are characterized by complex geometries resulting from the large number of buildings of varied shapes and dimensions. These obstacles strongly influence wind velocity since wakes, stagnating zones, recirculation, and preferential paths that may be present or arise can significantly complicate the scenario in simulations. Representing such complex geometries simply but realistically can prove cumbersome and often limit the utility of detailed simulation models.

Accidental releases of hazardous gases have been the subject of studies since the early 1980s and were investigated by the executing trials of large spills and development of numerical models; these models continue to be currently utilized for loss prevention purposes in chemical- and process industries [1,2], and some of them, like DEGADIS, SLAB, ALOHA, and UDM, are among the most popular and widely used models in safety engineering applications [3,4]. These are lumped-parameter models, usually pseudo one-dimensional, and account for some physical phenomena using semi-empirical relationships whose parameters have been tuned on field test data [5]. Since the experimental setup of these field trials usually does not involve any particular obstacle, these models can provide reliable results only in open field conditions, that is, when almost no obstacles are present in the cloud region.

To analyze the effects of multiple large obstacles on gas dispersion, computational tools based on computational fluid dynamics (CFD) can be utilized to simulate the complex urban geometries involved. This approach enables performing full three-dimensional analysis, and predicting velocity, temperature, and concentration

* Corresponding author. Fax: +39 0223993180.
E-mail address: renato.rota@polimi.it (R. Rota).

0304-3894/$ – see front matter © 2009 Elsevier B.V. All rights reserved.
doi:10.1016/j.jhazmat.2009.11.070

Nomenclature

c_p	constant pressure specific heat coefficient (J/kg K)
c_v	constant volume specific heat coefficient (J/kg K)
$C_{1,\varepsilon}$	k–ε model specific constant
$C_{2,\varepsilon}$	k–ε model specific constant
$C_{3,\varepsilon}$	k–ε model specific constant
C_μ	k–ε model specific constant
$\vec{g}$	gravitational acceleration (m/s^2)
G_b	turbulent generation term due to buoyancy (kg/m s^3)
G_k	turbulent generation term due to shear stress (kg/m s^3)
k	turbulent kinetic energy (m^2/s^2)
k_T	heat exchange coefficient (W/m K)
K	Von Karman constant
p	pressure (Pa)
S_ε	user-defined ε-generation term (kg/m s^4)
t	time (s)
T	temperature (K)
T_*	friction temperature (K)
u_i	i-th component of the velocity vector (m/s)
u_*	friction velocity (m/s)
$\vec{v}$	velocity vector (m/s)
x_i	i-th component of the coordinate vector (m)
Y_M	turbulent generation term due to compressibility (kg/m s^3)
z	height above ground (m)

Greek letters

ε	turbulent dissipation rate (m^2/s^3)
μ	molecular viscosity (kg/m s)
μ_T	turbulent viscosity (kg/m s)
ρ	density (kg/m^3)
σ_k	Prandtl number for k
σ_ε	Prandtl number for ε
$\bar{\bar{\tau}}$	stress tensor (N/m^2)
ϕ_m	semi-empirical function for atmospheric stability
ϕ_ε	semi-empirical function for atmospheric stability

fields in the integration domain. While this procedure might ensure more detailed results, it requires a large amount of resources both in terms of CPU time and analysts' skills.

Particular attention has to be paid in CFD simulations to turbulence modelling. The effect of turbulent fluctuations can be modelled by the RANS (Reynolds averaged Navier–Stokes) approach, or fully simulated by direct numerical simulation (DNS). The DNS places very large demands on resources and, nowadays, is applied only to very simple cases. An intermediate solution is to use large eddy simulations (LES) that simulate only larger eddies and use models for simulating the effects of isotropic dissipating eddies. Although LES is less demanding than DNS, it is still quite demanding in complex scenarios. Consequently, RANS remains a good compromise between result accuracy and computational efforts. The most popular closure model for turbulence effects in the frame of the RANS approach is the k–ε two-equation model, since it ensures reasonable results and good stability [6].

CFD results have been successfully validated against experimental field data [7,8] and lab-scale trials [9]. Some works have also been carried out in geometrically complex scenarios, involving few obstacles [10,11], or idealized urban canopies [12]. Realistic urban areas have been studied, analyzing the flow field in Hong Kong [13] and Manhattan [14]; in both these studies, flow of motions around buildings have been simulated while [15] the dispersion of a tracer gas has been also analyzed and the results obtained have been compared using integral models and hybrid models to assess concentrations in fields. However, where atmospheric stability was concerned, only wind-, temperature-, and turbulence profiles were imposed at the inlet boundary, without verifying whether the turbulence closure model maintains the profiles imposed at the wind inlet boundary throughout the integration field thereby assuring the correct representation of the physical phenomena involved.

In this work, realistic gas dispersion in a geometrically complex environment (i.e. urban terrain) was studied utilizing CFD tools, enabling a full 3D analysis of the effects of the obstacles in the impact area of the hazardous cloud. In particular, as a case study, ammonia dispersion was studied in the Lecco municipality, which is a small city located in a highly industrialized region in the north of Italy. The influence of the atmospheric stability was accounted for using the ASsM approach [16] which ensures consistency of the turbulence closure model with the Monin-Obhukov similarity theory. Moreover, since consequences of toxic gas dispersion mainly depend on the absorbed dose, a dedicated methodology was implemented in the CFD code for absorbed dose evaluation.

To represent simply but realistically the geometry of the urban buildings, a dedicated procedure was developed for the reconstruction of the 3D city model from the available topographic database and its direct import into the CFD code, since the realistic representation of all the buildings present in the integration domain represents one of the key problems when urban environments are involved.

Finally, the results obtained were compared with those computed using an integral dispersion model, commonly used in industrial risk assessment [3,4]. This enabled verification of the performance of integral models when dealing with complex environments.

2. Theoretical background

CFD codes solve Navier–Stokes Eqs. (1) and (2) together with specific model equations, such as energy balance (3), species diffusion, turbulence, etc.

$$\frac{\partial \rho}{\partial t} + \nabla \cdot (\rho \vec{v}) = 0 \tag{1}$$

$$\frac{\partial}{\partial t}(\rho \vec{v}) + \nabla \cdot (\rho \vec{v}\vec{v}) = -\nabla p + \nabla \cdot (\bar{\bar{\tau}}) + \rho \vec{g} \tag{2}$$

$$\frac{\partial (\rho c_v T)}{\partial t} + \nabla \cdot (\rho \vec{v} c_p T) = \nabla \cdot (k_T \nabla T) \tag{3}$$

In the equations above, ρ is the density, t the time, v the velocity, p the pressure, τ the shear stress, g the gravity acceleration, c_v and c_p the specific heats, T the temperature, and k_T the thermal conductivity.

In this work, the k–ε model was used to represent the effects of turbulence. This model introduces two additional transport equations for turbulent kinetic energy k (4) and turbulent kinetic energy dissipation rate ε (5), respectively [17]:

$$\frac{\partial}{\partial t}(\rho k) + \frac{\partial}{\partial x_i}(\rho k u_i) = \frac{\partial}{\partial x_j}\left[\left(\mu + \frac{\mu_T}{\sigma_k}\right)\frac{\partial k}{\partial x_j}\right] + G_k + G_b - \rho\varepsilon - Y_M \tag{4}$$

$$\frac{\partial}{\partial t}(\rho \varepsilon) + \frac{\partial}{\partial x_i}(\rho \varepsilon u_i) = \frac{\partial}{\partial x_j}\left[\left(\mu + \frac{\mu_T}{\sigma_\varepsilon}\right)\frac{\partial \varepsilon}{\partial x_j}\right] + C_{\varepsilon 1}\frac{\varepsilon}{k}(G_k + C_{\varepsilon 3}G_b) - C_{\varepsilon 2}\rho\frac{\varepsilon^2}{k} + S_\varepsilon(z) \tag{5}$$

where u_i is the velocity component along x_i direction, μ the viscosity, μ_T the turbulent viscosity, G_k the shear stress-related turbulent

kinetic energy production (6), G_b the buoyancy-related turbulent kinetic energy production (7), Y_M the compressibility-related kinetic energy production.

$$G_k = -\rho\overline{u_i' u_j'}\frac{\partial u_j}{\partial x_i} \tag{6}$$

$$G_b = \beta g_i \frac{\mu_t}{Pr_t}\frac{\partial T}{\partial x_i} \tag{7}$$

In Eqs. (6) and (7), β is the coefficient of thermal expansion, g_i is the component of the gravitational vector along x_i, Pr_t is the turbulent Prandtl number for energy and T the temperature. $C_{\varepsilon 1}$, $C_{\varepsilon 2}$, $C_{\varepsilon 3}$, σ_k, σ_ε, and C_μ are empirical constants. Jones and Launder [18] values were used for all the k–ε model constants. The commercial package Fluent 6.2.16 was used for all the computations.

As discussed elsewhere [16], the ASsM approach used to reproduce the effects of the atmospheric stability requires an additional source term, S_ε, to assure consistency between k–ε model predictions and Monin-Obhukov similarity theory profiles across the whole of the integration domain to enable a proper representation of different stability classes. Neutral stratification (8) and stable stratification (9) can be written as [16]:

$$S_\varepsilon(z) = \frac{\rho u_*^4}{z^2}\left[\frac{(C_{\varepsilon 2} - C_{\varepsilon 1})\sqrt{C_\mu}}{K^2} - \frac{1}{\sigma_\varepsilon}\right] - \mu\frac{u_*^3}{2Kz^3} \tag{8}$$

$$S_\varepsilon(z) = \frac{u_*^4\rho}{z^2}\left[\frac{(C_{\varepsilon 2} - C_{\varepsilon 1})\sqrt{C_\mu}}{K^2}\Phi_\varepsilon^2\sqrt{\frac{\Phi_\varepsilon}{\Phi_m}} - \frac{1}{\sigma_\varepsilon}\left(\frac{2}{\Phi_m} - \frac{1}{\Phi_m^2} + \frac{T_*}{KT}\right)\right] - \mu\frac{2u_*^3}{Kz^3} \tag{9}$$

A value of $C_S = 0.978$ for modelling the logarithmic profiles close to the walls was used to ensure consistency between the logarithmic profile and the approach for representing atmospheric stability classes, while fully developed vertical profiles of velocity, temperature, turbulence intensity, and dissipation rate were computed through periodic 2D simulations and used as boundary conditions at the wind inlet boundary [16]. Standard boundary conditions were used for other boundaries.

The reliability of the ASsM approach has been already discussed with reference to experimental data of field tests performed with or without obstacles within a domain [16].

Since in unsteady releases concentration profiles change over time, they cannot be directly used for risk assessment, that is, for evaluating individual risk and societal risk. For consequence analysis of this kind of scenario, Probit functions are often used to calculate the probability of death by the exposure to a toxic substance for a given time as [19]:

$$Pr = a + b\cdot\ln(D) \tag{10}$$

where $D = \int_0^\infty C^n dt$ is the toxic dose (C is the concentration of toxic gas, t is the time, and a, b, and n are parameters that depend on the gas involved). The relationship between the death probability P and the corresponding Probit value, Pr, is given by:

$$P = 0.5\left[1 + erf\left(\frac{Pr - 5}{\sqrt{2}}\right)\right] \tag{11}$$

The toxic dose, being an integral value, depends on the evolution of the gas cloud over time. Consequently, where stagnation zones exist, the dose grows even for small concentration values since in these regions the toxic gas remains for a long durations.

A specific methodology was implemented in the CFD code for evaluating toxic dose by initializing a specific field value which had been stored for each cell. A dedicated user-defined function (PROBIT tool) was developed, which reads the concentration value C and the time-span of the unsteady simulation interval time, Δt. Therefore, $C^n\cdot\Delta t$ value can be calculated and is added to the D value computed for each cell at the previous time step. The integral value of the toxic dose is, therefore, reduced to a sum of discrete contributions characterized by constant concentrations of hazardous gas. The sensitivity of the results on the time step was checked in order to obtain a solution that is not dependent on time discretization. From the dose value, the Probit function value can then be easily computed for each cell.

Finally, for the sake of comparison the same computations carried out with the CFD code were repeated using an integral model, namely the UDM, implemented with the commercial PHAST model suite [20].

Table 1
Major atmospheric parameters used in all the computations.

	D5	F2
Wind speed ($m\,s^{-1}$)	5	2
Stability class	D	F
Reference height (m)	2	2
Temperature (°C)	27	20
Ground temperature (°C)	27	18
Surface roughness (m)	0.006	0.006
Monin-Obhukov length (m)	∞	9

3. Accidental scenario definition

In order to reproduce a realistic accidental scenario, the released material was chosen from among the major hazardous products that are usually transported through the Lecco municipality [21]. Therefore, a catastrophic rupture of a typical tank truck transporting ammonia-water solutions (10%, w/w) with a capacity of about 10,000 kg was considered, resulting in a pool of about 36 m diameter and an evaporation rate of about 7.8 and 3.6 $kg\,s^{-1}$, and an average pool temperature of about 11 and 8 °C, as computed by standard models for the two atmospheric conditions considered, namely D5 and F2. This means neutral stratification with wind speed, at a reference height of 5 $m\,s^{-1}$ and stable stratification with wind speed of 2 $m\,s^{-1}$. These are the most widely used atmospheric conditions in risk assessment since they usually involve serious consequences: stable stratification means a small amount of atmospheric turbulence, therefore, a small amount of air is entrained in the gas cloud; neutral stratification, while characterized by a greater amount of turbulence, is usually characterized by greater wind velocity, and, consequently, by faster spread of the cloud. Unstable stratification (stability class among A and C) involves a substantial amount of atmospheric turbulence; the air entrainment increases and the resulting impact area, therefore, is greatly reduced. The main atmospheric parameters for these conditions are summarized in Table 1.

Wind direction was set as that prevalent during the daytime.

Ammonia evaporation was simulated with the CFD code through a diffusive flux from a pool with constant radius and temperature, using the aforementioned average values.

Probit constants for ammonia, used in all the numerical simulations were $a = -16.14$, $b = 1$, and $n = 2$ [19].

4. Construction of the urban 3D model

The reconstruction of the so-called *3D city model* and its import into the CFD code represents one of the key aspects of the approach adopted in this study for modelling gas dispersion in urban environments. In recent years, several techniques have been developed

to provide different kinds of data sources to build up such models, which are mostly based on airborne sensors like analogue and digital aerial cameras, and LiDARs [22]. Techniques used for commercial mapping are still currently based on *aerial photogrammetry* (AP): a block of images acquired through an aerial digital camera (or alternatively by an analogue camera followed by scanning to obtain digital imagery) is then processed by means of a procedure that today is highly automated. After the image *orientation*, i.e. the reconstruction of the position and altitude of each photo at the moment of capture, a map is derived through *stereo-plotting*, a process which exploits the 3D stereoscopic view obtainable from a pair of overlapping images. Stereo-plotting is operated by an expert technician with a low level of automation. AP-based maps are usually made up of prevalently planimetric objects which are integrated by information on their elevation. They are recorded in vector form and stored in CAD or GIS data formats. But stereo-plotting also allows the direct derivation of 3D city models that are made up of a more complete reconstruction of the urban environment, where buildings are accurately modelled and photo-textures might be added up. The production of such models may take advantage of *oblique aerial photos* (see examples at http://www.bing.com/maps/ www.local.live.com for the most large towns in Western Europe or the United States) rather than traditional *nadir* imagery (those captured with the camera plane parallel to the object on the ground and looking downwards) which are routinely adopted in AP. Oblique photos enable a better reconstruction of the whole 3D building model and are not limited to the ground perimeter and the roof only. Considering their complex structures, these may require specific informatic formats to be stored [23].

Accordingly, to provide a 3D city model as boundary constraint to the gas dispersion problem, an AP product was chosen, which fulfilled several key constraints, such as:

having standard properties, format and diffusion, so that the method can be extended to a wider area;
easy handling and manageability, especially when dealing with the 3D model extraction from the original data;
featuring an appropriate level of detail (LoD), considering also limitations in computing machines when running CFD codes;
having public diffusion at free or low cost; this criterion rejects, for instance, the use of 3D city models used by mobile phone companies, which are widely widespread across Europe.

These criteria have driven the adoption of the *topographical database* (TDb), which is a spatial data infrastructure (SDI) obtained from AP whose basic principles have been defined by a national commission [24]; the EUINSPIRE directive [25] has been followed in setting up the TDb structure. The Regional Administration of Lombardia region, where the case study of Lecco is located, published a set of technical specifications that draw the structure and the content of TDbs which are commonly used by municipalities for urban planning purpose. It is predicted that in a few years (approximately 3–4) the whole regional coverage, integrated by digital orthoimages and Digital Terrain Models (DTMs) will be available. The LoD and the mapping tolerances reported in Table 2 for all scales are appropriate for urban modelling required by gas dispersion simulations, considering that urban settlements are usually represented with a TDb-2k (i.e. at 1:2,000 scale).

The TDb is delivered free of cost by the Municipality of Lecco city in a well known GIS data format (*Shapefile*® ESRI, USA). Specifications enumerate all Classes of objects to be represented with a given geometric feature (point, arc, area). For example, a building is described by an area, a creek with width under the capture limit by an arc, and a lighting pole by a point. Each vertex has a planimetric coordinate in the mapping coordinate system (UTM grid based on geodetic coordinates WGS84-ETRF89) and orthometric height as well; information on the Italian grids and datum can be found in Mugnier [26]. All objects are then three-dimensional, even though most of them are represented with the height of their contour at the ground level. Each object of the TDb is linked to a record of a Db (*attribute table*), where further information on it is archived. Apart from some codes to classify the object Class the feature belongs to, each record always contains an identifier (*Id*) which distinguishes it from the other objects of the same Class, and some additional attributes like the mean height of a building.

Table 2
LoD expressed as capture limit (i.e. the largest linear or areal extension of an object to be represented in scale into the TDb) and mapping tolerances (at 95% confidence level) for the TDb framework defined by Lombardia region technical specifications.

	1k (m)	2k (m)	5k (m)	10k (m)
Capture limit	0.3	0.6	1.5	3.0
Tolerances				
Position	0.6	1.2	3.0	6.0
Elevation	0.6	0.8	2.0	4.0

Therefore, the TDb is not real 3D cartography but contains data to build up a 3D city model. This task can be easily performed by using standard functions in a *desktop GIS* environment like ArcGIS® 9.2 (or following) with ArcScene® module (ESRI, USA). The workflow that was setup to yield the 3D model was made up of the following steps:

1. *Selection of the object classes*: Not the whole content of TDb is needed to derive the 3D city model, but only those Classes that contribute to defining the 3D geometry. Classes to be used must give the *complete ground coverage* (CGC), i.e. each area has to be covered by only one feature without any discontinuity.
2. *Spatial query on the interested area to exclude external data*: The TDb is organized in datasets covering a specific area, in this case the entire land mass within the Municipality of Lecco. The case study being limited to a portion of this, a *spatial query* is applied to remove external data.
3. *Construction of the TIN for ground modelling*: All vertices of objects comprising the CGC are used to built up the TIN (*Triangulated Irregular Network* [27]) which defines the ground level of the 3D city model. Perimeters of all constructions are constrained to be nodes of the TIN, in order to keep spatial coherence between the soil and the building models.
4. *Extrusion of countours to reconstruct the main body of buildings*: The features Class describing the geometry of a building is provided with the elevation a.s.l., complemented by a field of the *attribute table* expressing their relative heights from the ground to the roof edge. By operating the ArcScene® 9.2 environment, buildings are extruded to 3D prisms to yield a rough 3D model which, however, is still appropriate as an input for CFD codes.
5. *Modelling of roofs*: The rough model obtained, as described in the previous item (4), can be further improved by roof modelling if roof slopes, roof edges, and lines of the eaves are included into the TDb. Usually, this happens when a TDb-1k is available (1:1,000 scale), as it happened in the case study area. However, the actual structure of TDb does not contain information on roof slopes, which should be derived from edges and lines of the eaves by developing suitable macros [28], or by manual editing in the case of small datasets.
6. *3D model editing and export*: The 3D model needs to be visually inspected to detect gaps in both horizontal and vertical continuity. Where detected, these must be filled by editing some additional features or by recovering data from the original TDb. A topological analysis to detect discontinuities could be useful, because small gaps might not be detected by mere visual inspection of the model. Finally, the 3D model requires to be exported

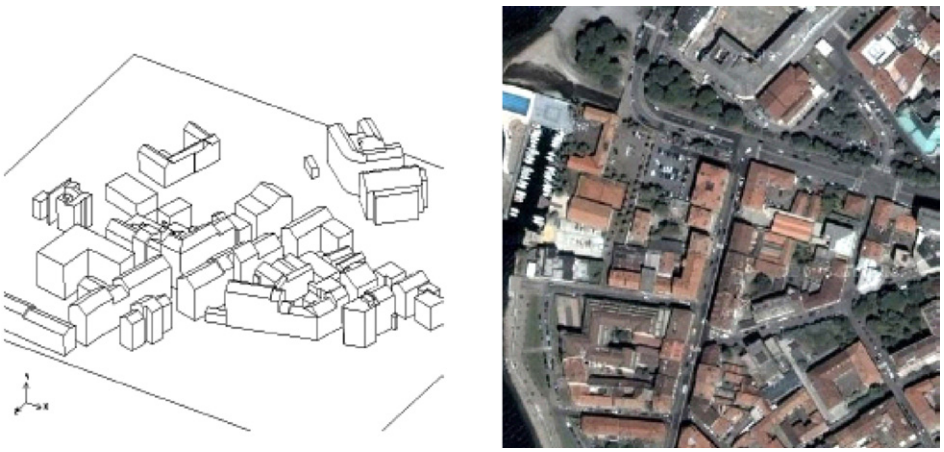

Fig. 1. A 3D visualization of a portion of the TDb-1k of the case study area in Lecco city, with an orthoimage of the same area.

in a format that can be directly imported into the mesh-building software. In this case, the standard IGES format was successfully adopted. The imported data was cleaned up to remove small details which had minor influence on the gas dispersion related to cell refinement they require. The minimum detail level considered was about 20 [cm].

In Fig. 1, a portion of the TDb of Lecco town is shown with an aggregate orthophoto of the same area. This integration domain was about 300 m length, 250 m depth, and 100 m height and involved about 1500k cells, which was enough to provide grid-independent results.

5. Results and discussion

Figs. 2 and 3 represent the iso-concentration values of ammonia for ERPG I (25 ppm), ERPG II (200 ppm), and ERPG III (1000 ppm) for D5 and F2 conditions, respectively. We can see that there are no large differences between the two atmospheric stratifications since the buildings interfere with wind velocity, providing a flow field mainly characterized by the urban canopy and loosely dependent on atmospheric wind profile. As a consequence, ammonia concentration rises in the wakes of buildings, where wind speed is smaller and recirculation time becomes greater and is depleted where fresh air is canalized by the obstacles and entrained in the cloud.

The obstacles also interfere on the source term. As shown in Table 3, for both neutral- and stable stratifications wind velocity is reduced by about ten times that of open field conditions (that is, where there are no obstacles), since the pool was situated just downwind of a building. Nevertheless, the evaporation rate shows an opposite trend for the two conditions: it decreases for neutral stratification and increases for stable stratification with respect to open field conditions. This is explained by the turbulence effect related to building wake: while in D5 stratification the decreasing of the wind speed plays a major role in obstacle wake and leads to a decrease of the turbulent kinetic energy near the pool, in F2 stratification since the initial atmospheric turbulence is much smaller, the turbulence source term due to the wake of the building becomes the most important contribution, raising the turbulent kinetic energy near the pool.

Higher values of turbulent kinetic energy mean higher dispersion coefficients and, consequently, larger diffusive flux. Since ammonia evaporation was modelled through a diffusive flux, this means a larger evaporation rate in F2 conditions. On the other hand, a smaller turbulent kinetic energy value leads to a smaller diffusive flux, and therefore to a smaller evaporation rate in D5 conditions.

Table 3
Effect of the urban environment on the source term. Wind speed and turbulent kinetic energy are measured at the centre of the pool, 1 m above the pool surface.

D5	CFD, open field	CFD, urban terrain
Wind speed ($m\,s^{-1}$)	4.1	0.7
Turbulent kinetic energy ($m^2\,s^{-2}$)	0.3	0.2
Evaporation rate ($kg\,s^{-1}$)	7.8	7
F2	CFD, open field	CFD, urban terrain
Wind speed ($m\,s^{-1}$)	1.6	0.16
Turbulent kinetic energy ($m^2\,s^{-2}$)	0.06	0.07
Evaporation rate ($kg\,s^{-1}$)	3.6	4.5

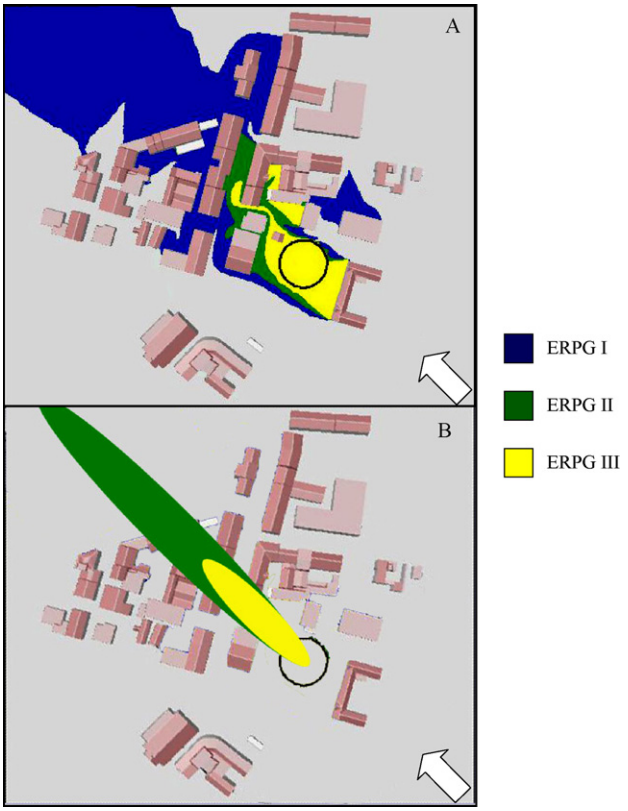

Fig. 2. Ammonia iso-concentration contours (ERPG I, II, and III) predicted by CFD (A) and integral model (where the ERPG I contour has been omitted since it exceeds the domain dimensions) (B) in D5 conditions. White arrows represent wind direction, black circle the pool position.

Starting from the same computations, the PROBIT values could also be predicted, as shown in Figs. 4 and 5.

For PROBIT values, such as for ammonia iso-concentrations, influence of buildings plays a major role and dependence upon atmospheric turbulence is consistently reduced. PROBIT value is enhanced by building wakes, zones where recirculation takes place; in particular, the upwind diffusion of the gas with the consequent formation of high PROBIT areas should be noted.

Figs. 2–5 also report the predictions of the integral model for both ERPG and PROBIT values. For D5 stratification, the ERPG III maximum distance predicted by integral model simulations is comparable with CFD model predictions, while ERPG II is much larger. These results depend on two overlapped effects: buildings act as obstacles creating stagnation zones, slowing the wind velocity and, consequently, reduce the flow turbulence near the ground where the shear stress effect otherwise prevails; on the other hand, they create recirculations and eddies, increasing the turbulence away from the ground boundary layer. Consequently, gas dispersion is slowed near the pool, where the cloud of ammonia is close to the ground, and is directed away from the source term.

With F2 stratification, open field simulations showed that the wind speed is not high enough to bend the ammonia cloud (whose density is lower than that of the surrounding air) to the ground; consequently the integral model predicts PROBIT and ERPG values all within the pool radius, except for ERPG I, which reaches a distance of about 40 m. In CFD simulations, the cloud is intercepted by buildings and recirculation takes place in the urban canyons; ammonia is, therefore, forced near the ground by this recirculation, where the reduced wind speed and turbulent intensity make dispersion slower, as shown for the sake of illustration in Fig. 6.

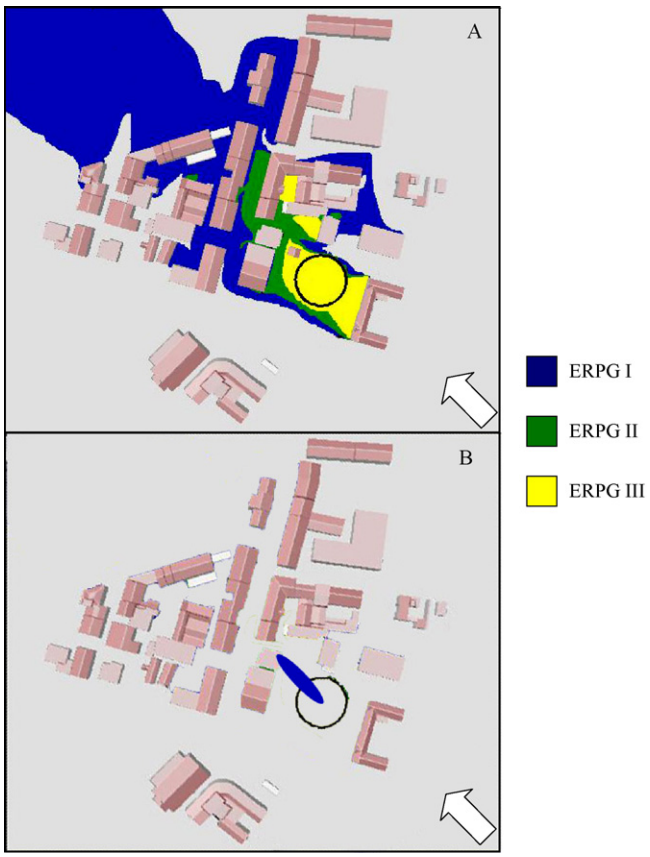

Fig. 3. Ammonia iso-concentration contours (ERPG I, II and III) predicted by CFD (A) and integral model (B) in F2 conditions. White arrows represent wind direction, black circle the pool position.

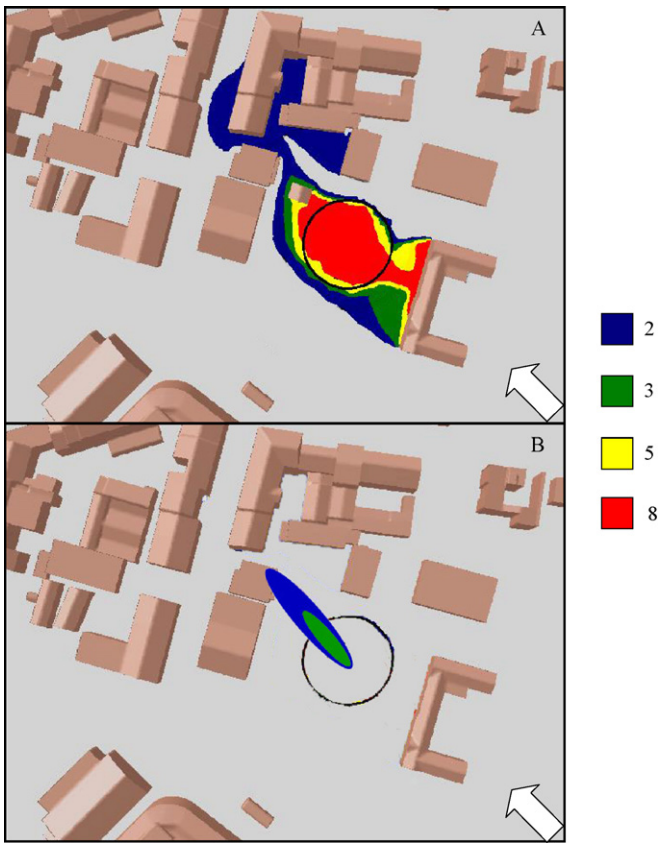

Fig. 4. Regions affected by death probability higher than 0.1% (PROBIT > 2), 2% (PROBIT > 3), 50% (PROBIT > 5), and 99.9% (PROBIT > 8) as predicted by CFD (A) and integral model (B) in D5 conditions. White arrows represent wind direction, black circle the pool position.

It should be noted that the highly concentrated stream of ammonia blowing over the buildings is bent by the building wakes, thus the ammonia is channelled towards the ground. Once it has reached the bottom of the urban canyon, the effect of the obstacles that start prevailing on atmospheric stratification and gas dispersion in F2 conditions becomes comparable with the behaviour of the gas observed in D5 conditions. Obviously, the integral models did not take into account the influence of full 3D obstacles and, consequently, they could not predict this feature.

For D5 conditions, while the integral model overestimates the distance reached by ERPG II, it underestimates the hazardous area

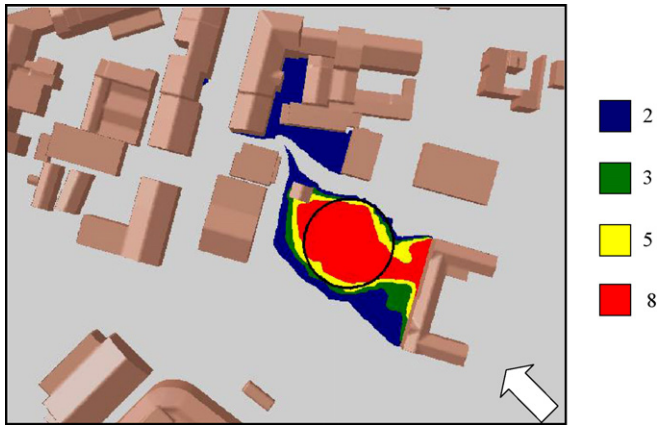

Fig. 5. Regions affected by death probability larger than 0.1% (PROBIT > 2), 2% (PROBIT > 3), 50% (PROBIT > 5), and 99.9% (PROBIT > 8) as predicted by CFD in F2 conditions. White arrows represent wind direction, black circle the pool position.

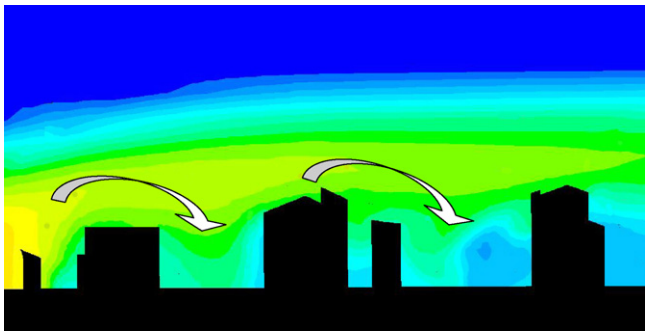

Fig. 6. Ammonia transport towards the ground by building wakes.

in terms of death probability; this is caused by the presence of a large recirculation zone created by the buildings. Moreover, the integral model cannot predict upwind gas dispersion, which however takes place creating a zone characterized by a high PROBIT value.

For F2 stratification, the differences between the two approaches grow even larger, due to the canyon recirculation previously referred.

Finally, Fig. 7 shows the ammonia iso-concentration contours predicted using CFD tools with a standard k–ε turbulence model (that is, without the ASsM approach), for both D5- and F2 conditions. Comparing these results with those reported in Figs. 2(A) and 3(A), we can see that in D5 stratification the predictions obtained with a standard k–ε turbulence model are quite acceptable. In neutral stratification, the shear stress plays a major role in turbulence production and it is well modelled by the standard k–ε turbulence model. In F2 stratification, instead, the buoyancy contribution in reducing atmospheric turbulence is not negligible; the standard k–ε could not properly handle this contribution leading to a more turbulent solution and, consequently, to smaller areas identified by the previously defined iso-concentration values. In particular, it should be noted that the ERPG III contour is practically limited to the pool size, and no high concentration stagnation zones are predicted in the other regions of the investigated domain.

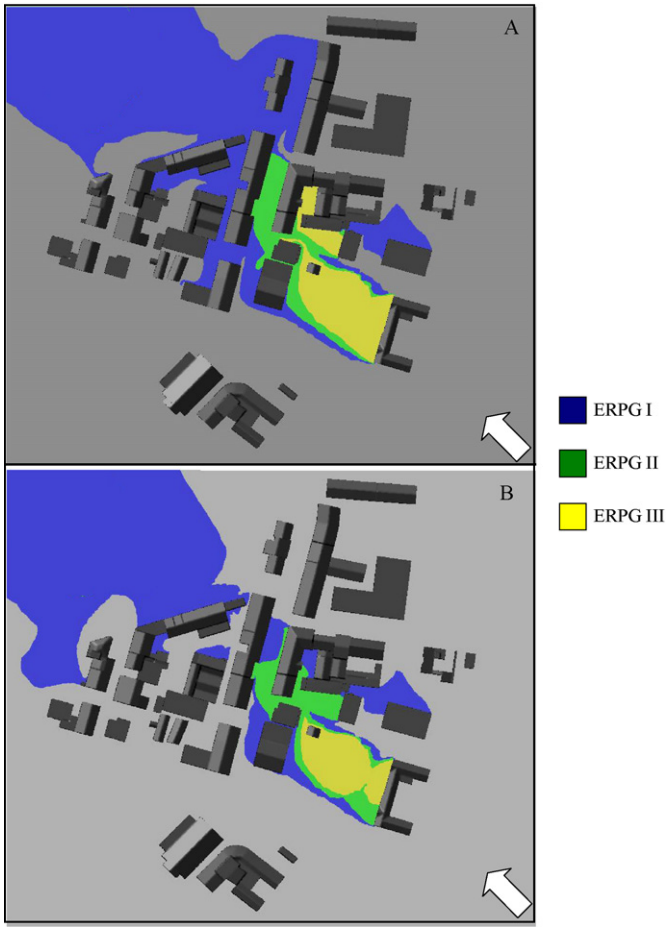

Fig. 7. Ammonia iso-concentration contours (ERPG I, II, and III) predicted by CFD with standard k-ε turbulence model in D5 (A) and F2 conditions (B). White arrows represent wind direction.

6. Conclusions

In this work it has been shown, using a previously validated CFD model, that using integral models in environments with complex geometries can either overestimate or underestimate the consequences of a major accident. This should be properly considered by safety engineers and decision makers.

As a consequence, a new methodology for risk assessment related to the release of hazardous products in geometrically complex environments has been developed. It involves the use of a CFD model together with:

- a simple and fast technique to import complex 3D geometries in a CFD simulation tool from topographic databases, which allows for a simple but very detailed analysis of the geometry of all the buildings present in a real urban environment;
- the ASsM approach for accounting of atmospheric stability, which allows for analyzing realistic atmospheric stability classes;
- a new submodel for the evaluation of the absorbed dose of a toxic compound, which allows for using Probit analysis together with CFD simulations.

Finally, to confirm its practical applicability, the proposed methodology has been applied to a case study involving a major accident related to the transport of hazardous material in a town in the north of Italy.

Acknowledgements

Financial support of the iNTeg-Risk project (contract number NMP2-LA-2008-213345) of the 7th Framework Programme of the European Commission, as well as that of the Italian MIUR – PRIN2007 are gratefully acknowledged.

References

[1] M. Nielsen, S. Ott, A collection of data from dense gas experiments, RISO Report R-845(EN) RISO, Roskilde, 1996.
[2] S. Hanna, R. Britter, Wind Flow and Vapor Cloud Dispersion at Industrial and Urban Sites, CCPS, New York, 2002.
[3] A. Bernatik, M. Libisova, Loss prevention in heavy industry: risk assessment of large gasholders, J. Loss Prevent. Proc. Ind. 17 (2004) 271–278.
[4] D.R. Brook, N.V. Felton, C.M. Clem, D.C.H. Strickland, I.H. Griffiths, R.D. Kingdon, Validation of the urban dispersion model (UDM), Int. J. Environ. Pollut. 20 (2003) 11–21.
[5] J.S. Nordin, Practical uses of air plume modelling in chemical emergencies, in: M. Fingas (Ed.), The Handbook of Hazardous Materials Spills Technology, McGraw-Hill, New York, 2002, pp. 17.1–17.18.
[6] A. Luketa-Hanlin, R.P. Koopman, D.L. Ermak, On the application of computational fluid dynamics codes for liquefied natural gas dispersion, J. Hazard. Mater. 140 (2007) 504–517.
[7] S. Sklavounos, F. Rigas, Simulation of Coyote series trials, part I: CFD estimation of non-isothermal LNG releases and comparison with box-model predictions, Chem. Eng. Sci. 61 (2006) 1434–1443.
[8] B.R. Cormier, R. Qi, G.W. Yun, Y. Zhang, M.S. Mannan, Application of computational fluid dynamics for LNG vapor dispersion modeling: a study of key parameters, J. Loss Prevent. Proc. Ind. 22 (2009) 332–352.

[9] M.A. McBride, A.B. Reever, M.D. Vanderheyden, C.J. Lea, X.X. Zhou, Use of advanced techniques to model the dispersion of chlorine in complex terrain, Proc. Safety Environ. Prot. 79 (2001) 89–102.
[10] H.A. Olvera, A.R. Choudhuri, W.W. Li, Effects of plume buoyancy and momentum on the near-wake flow structure and dispersion behind an idealized building, J. Wind Eng. Ind. Aerod. 96 (2008) 209–228.
[11] P. Neofytou, A.G. Venetsanos, D. Vlachogiannis, J.G. Bartzis, A. Scaperdas, CFD simulation of the wind environment around an airport terminal building, Environ. Modell. Softw. 21 (2006) 520–524.
[12] D. Schmidt, U. Krause, U. Schimidtchen, Numerical simulation of hydrogen gas releases between buildings, Int. J. Hydrogen Energy 24 (1999) 479–488.
[13] Y. Yang, Y. Shao, Numerical simulations of flow and pollution dispersion in urban atmospheric boundary layers, Environ. Modell. Softw. 23 (2008) 27–40.
[14] S.R. Hanna, M.J. Brown, F.E. Camelli, S.T. Chan, W.J. Coirier, O.R. Hansen, A.H. Huber, S. Kim, R.M. Reynolds, Detailed simulations of atmospheric flow and dispersion in downtown Manhattan: an application of five Computational Fluid Dynamics models, Bull. Am. Meteorol. Soc. 87 (2006) 1713–1726.
[15] B. Blocken, T. Stathopoulos, J. Carmeliet, CFD simulation of the atmospheric boundary layer: wall function problems, Atm. Environ. 41 (2007) 238–252.
[16] M. Pontiggia, M. Derudi, V. Busini, R. Rota, Hazardous gas dispersion: a CFD model accounting for atmospheric stability classes, J. Hazard. Mater. 171 (2009) 739–747.
[17] Fluent 6 User's Guide, Fluent Inc., Lebanon, 2006.
[18] W.P. Jones, B.E. Launder, The prediction of laminarization with a two-equation model of turbulence, J. Heat Mass Transfer 15 (1972) 301–314.
[19] TNO, Methods for the Determination of Possible Damage—The Green Book, CPR 16E, The Hague, 1989.
[20] A. Holt, H.W.M. Witlox, Validation of the unified dispersion model, Fluent technical reference manual, v.6.0, DNV, London, 1999.
[21] Provincia di LECCO – Settore Viabilità e Protezione civile, PIANO DI PROTEZIONE CIVILE, Studio per la determinazione del rischio viabilistico con particolare riferimento al trasporto di merci pericolose (in italian).
[22] K. Kraus, Photogrammetry—Geometry from Images and Laser Scans, Walter de Gruyter, Berlin, 2008.
[23] T.H. Kolbe, G. Gröger, L. Plümer, CityGML—3D city models and their potential for emergency response, in: S. Zlatanova, J. Li (Eds.), Geospatial Information Technology for Emergency Response, Taylor & Francis, London, 2008, pp. 257–274.
[24] Comitato per il coordinamento informatico dei dati territoriali (CNIPA), Italian Government (2008), http://www.cnipa.gov.it/site/it-IT/Attivit%c3%a0/Sistemi_Informativi_Territoriali/Specifiche_tecniche/, last accessed on 27th December 2008 (in Italian).
[25] European Union (2007), Directive 2007/2/EC.
[26] C.J. Mugnier, Grids & Datums, Italian Republic, Photogramm. Eng. Remote Sensing 8 (2005) 889–890.
[27] C. Jones, GIS and Computer Cartography, Prentice Hall, New York, 1997.
[28] G. Forlani, C. Nardinocchi, M. Scaioni, P. Zingaretti, Complete classification of RAW LIDAR data and 3D reconstruction of buildings, Pattern Anal. Appl. 4 (2005) 357–374.